Bulletin of Earthquake Engineering (2022) 20:7641–7674
https://doi.org/10.1007/s10518-022-01500-1

ORIGINAL ARTICLE

Numerical and analytical methods for the design of beam-column sub-assemblies with composite deck slab

Tushar Chaudhari[1] · Gregory MacRae[2] · Des Bull[2] · G. Charles Clifton[3] · Stephen J. Hicks[4]

Received: 2 February 2022 / Accepted: 15 August 2022 / Published online: 1 September 2022

Abstract
A finite element numerical model is used to estimate the force displacement backbone curve of steel moment frame beam-column-joint subassemblies tested at large scale under repeated cyclic loading with different composite deck slab configurations. The slab configurations included: no-slab; fully isolated slab; two configurations for detailing the slab near the region between the column flanges; and a full depth reinforced slab. Then, a simple analytical model was developed so that designers can estimate the likely peak strength due to slab effect. This analytical model considers the common deformation modes and the strength hierarchy. It was found that the finite element numerical model captured the backbone envelope of experimental tests done on different slab configurations for the bare frame, isolated slab and full depth slab configurations, but overestimated the strength at larger displacements for the other configurations due to difficulty in considering the slab modes of failure. The simple analytical model considered the nonlinear deformation modes of steel beam plastic hinging, concrete crushing both outside the column flange and within the beam flanges, slab shear fracture between the column flange tips, slab longitudinal and lateral reinforcement yielding as it carried the subassembly moments and transferred forces between the steel frame and the slab, and shear stud deformation. The proposed analytical model matched the experimental strengths and failure modes. The proposed finite element model is suitable for research, and the analytical model matched the experimental results, and is suitable for consideration in design.

Keywords Force transfer mechanism · Micro model · Moment frames · Shear studs · Structural steel · Composite slabs

1 Introduction

Steel framed structures with composite slabs are popular in many seismically active regions around the world. Following the 2010–2011 Canterbury earthquakes, the number of steel-framed buildings with composite deck slabs in New Zealand has dramatically increased because of their: proven seismic performance; architectural flexibility;

✉ Tushar Chaudhari

Extended author information available on the last page of the article

ability to be easily connected, prefabricated, deconstructed and recycled; rapid construction time; and economy (Bruneau et al. 2010). Such steel frame buildings with the composite deck slabs can also easy to incorporate the new low-damage seismic resisting technology (MacRae and Clifton 2015) further increasing their sustainability.

In composite construction, both the concrete and steel material are effectively utilised by taking advantage of the concrete's compression properties and the steel's tensile properties. The beam-slab composite action is achieved using the steel shear studs welded onto the steel beam and embedded within into the concrete slab, resulting in the neutral axis being in the beam top flange or slab depending on the configuration and the degree of composite action (Johnson and Molenstra 1991; Oehlers and Bradford 1995).

In many cases, the composite beam (consisting of the steel beam and slab) is designed for gravity and the beam size may be governed by deflection. However, under seismic loading, where peak flexural demands occur at the beam ends, the slab effect is generally ignored, even though it may significantly influence the seismic performance (MacRae et al. 2013; Hobbs et al. 2013). New Zealand is unusual in that while slab effects are ignored for beam design, they are considered when considering the composite beam overstrength in earthquake design, and this affects the design of the panel zone and columns (MacRae et al. 2007; NZS3404:Part1: 1997).

Civjan et al. (Civjan et al. 2001), Leon et al. (Leon et al. 1998), Lee and Lu (Lee and Lu 1989), and Hobbs et al. (Hobbs et al. 2013) have shown that slab may increase the sub-assembly strength by more than 50%. Such increases may change a building deformation mode from being a strong column-weak beam to a strong beam-weak column mechanism if they are not properly considered (Leon et al. 1998). This can be undesirable with a greater likelihood of collapse (Yamada et al. 2009). Past steel building/subassembly research (Civjan et al. 2001; Leon et al. 1998; Lee and Lu 1989; Hobbs 2014) indicates a rapid post-peak strength degradation may be associated with concrete slab brittle failure at the column, and the final subassembly strength becomes that of the bare frame alone. The strength degradation rate depends on the force demand, force transfer mechanism strength hierarchy, and deformation compatibility. At lower lateral drifts there is no damage, but as drifts increase composite slab concrete microcracking occurs due to bearing failure in front of the column flange. At greater drifts, slab concrete crushing/spalling occurs at this location because the slab is not confined on the top. As drifts further increase, brittle shearing failure of the slab may occur between the column flange tips. Also, if the slab longitudinal shear strength is too low, this mechanism may occur before some of those above (Hobbs 2014).

Composite deck slabs are poured up to, and against, the steel columns in conventional construction practice. In this case, due to lateral forces on the frame, the slab bears against the column flanges on the sagging moment side and transfers the interaction forces primarily through the bearing on the column flanges. However, on the hogging side, the force transfer largely depends on the activation of the strut-and-tie mechanism (Plumier and Doneux 2001; Salvatore et al. 2005; EN1998-1 2004; Umarani and MacRae 2007). The force transfer between the concrete slab and column which must be considered in the column design, which is a function of the (i) concrete strength, (ii) slab confinement, (iii) column-slab contact area, (iv) number and location of beam shear studs, and the (v) provision of additional reinforcement for the strut-and-tie mechanism (Chaudhari et al. 2015).

In order to avoid slab effects on beam overstrength, some engineers are providing a gap between the slab and the steel column (MacRae et al. 2013; Hobbs 2014). This avoids the slab degradation, but there is a detailing cost. An alternative is providing a full depth slab

detailed so that it does not degrade in strength during seismic motions and a smaller steel beam may be used.

Based on the above discussion, there is a need to better understand the slab interaction effects in steel moment-frames with conventional slabs, isolated slab, or full depth slab considerations, and to be able to analyse their performance so that appropriate design decisions can be made. This paper seeks to address this need by seeking answers to the following questions:

(i) Does numerical simulation, using finite element analysis of the beam-column subassembly, capture the force transfer mechanisms associated with slab-column interaction?
(ii) Can simple hand calculation methods be used to estimate composite beam-column slab subassemblies lateral strength and stiffness?
(iii) What modes of deformation control subassembly strength?
(iv) What are the implications of the findings of this work for design?

2 Slab-column interaction and failure modes

Figure 1 explains two force transfer mechanisms between the slab and joint defined by Eurocode EN1998-1 (2004), as well as possible modes of failure within the slab-column interaction zone. The first lateral force resisting mechanism, Mechanism 1, involves direct compression from the slab on the outside of the column flanges, while Mechanism 2 involves compression on the inside of the column flange and inclined concrete compression struts. A third mechanism, Mechanism 3, also exists as a result of out-of-plane beam shear studs causing the top of the beam to move, thereby inducing beam torsion, and in-plane joint moment. While in many cases the contribution of force transfer from this mechanism is small, (Webb et al. 2018) it is discussed further here.

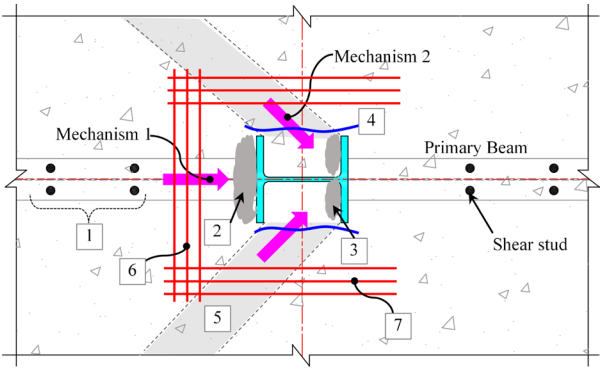

Fig. 1 Slab-column interaction zone and major deformation modes

Load paths for the slab to contribute to the frame sub-assembly lateral strength are as follows:

a. Load path 1 (LP1, involving Mechanism 1 as shown in Fig. 2a): Force is carried by the shear studs on the left-hand side of the column (i.e. sagging side) (mode 1) as they carry force from the slab to the beam (mode 5), and by the concrete at the column outer flange-slab interface (mode 2),
b. Load path 2 (LP2, involving Mechanism 1 as shown in Fig. 2b): Force is carried by mode-2, mode 5, and tie reinforcement tension (modes 6 and 7) and then through the shear studs on the right-hand side of the column (i.e. hogging side) (mode 1).
c. Load path 3 (LP3, involving Mechanism 2 as shown in Fig. 2c): Force is carried on the inside of the flanges (mode 3), and force must pass (mode 5) through the line between the flange tips (mode 4), and transverse reinforcement tension (mode 6) and then to the shear studs on the left-hand side of the column (i.e. sagging side) (mode 1).
d. Load path 4 (LP4, involving Mechanism 2 as shown in Fig. 2d): Force is carried by mode 3, mode 5, mode 4, and transverse and lateral reinforcement tension (modes 6 and 7) and then to the shear studs on the right-hand side of the column (i.e. hogging side) (mode 1).

Also, load paths can also act in parallel. If elements of the load path, associated with the different modes are not strong enough, then strength loss may occur. The strengths of the different modes are controlled by the actions as shown at the bottom of Fig. 1.

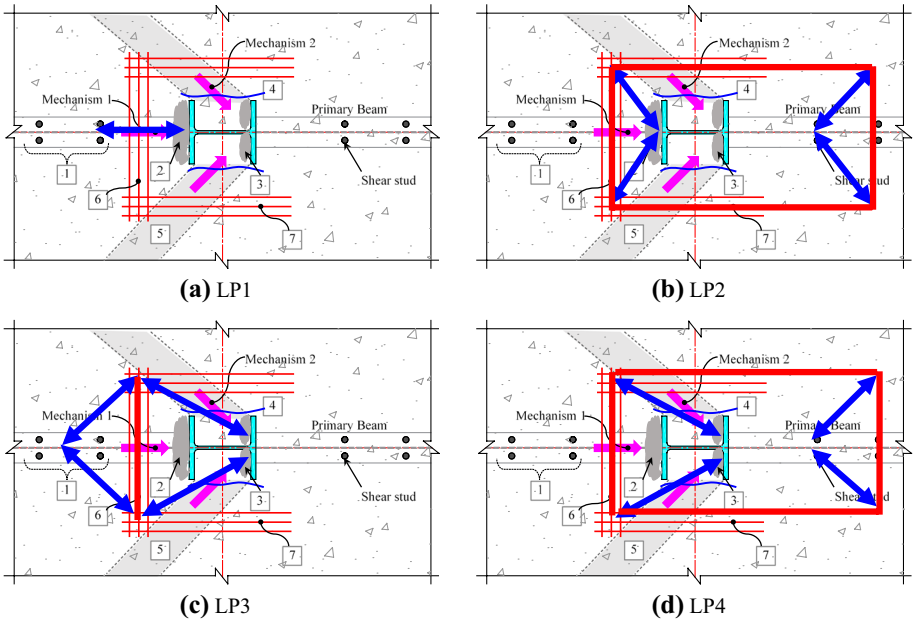

Fig. 2 Load paths for slab internal forces (red: tension, blue: compression)

3 Numerical methodology

3.1 Finite element model—geometry idealisation

The moment frame internal beam-column subassembly with composite deck slab shown in Fig. 3 was considered based on experimental tests of Chaudhari (Chaudhari 2018). This subassembly was designed using capacity design principles to obtain strong column/connection–weak beam behaviour so that the column remains elastic. The tested frame subassembly was modelled in ABAQUS (version 6.11.2) (Simulia 2011) in 3-D. Beam (310UB32 Grade 300), column (310UC198 Grade 300), continuity plates, gusset plates, metal deck, and column continuity plate members, as shown in Fig. 3a, consisted of four-noded shell finite elements (S4R) (Mago and Clifton 2008). The beam-to-column connection was modelled as rigid, without explicit consideration of the end-plates and bolts (Chaudhari et al. 2019), this is based on the experimental study conducted at the University of Canterbury and no damage to end-plate connection, panel zone or column was observed in any of the tests as these elements were designed to remain elastic. Also, the numerical model without the joint flexibility (SAP2000 model, (Chaudhari 2018)) gave similar behaviour to the experimental model.

The concrete slab was modelled using eight noded solid elements (C3D8R), and the reinforcing steel was modelled using the two noded beam elements (B31).

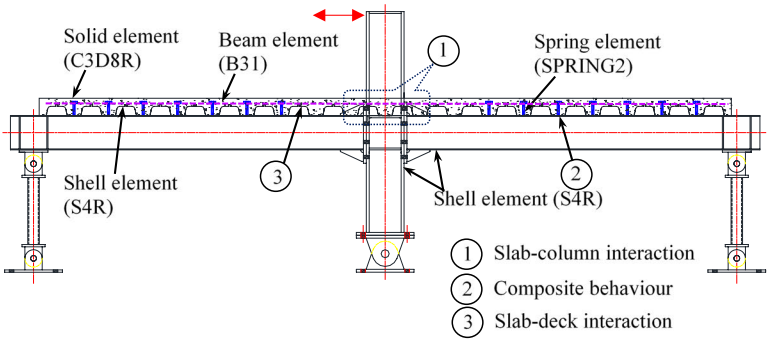

(a) Numerical Model Idealization of Tested Frame Sub-assembly.

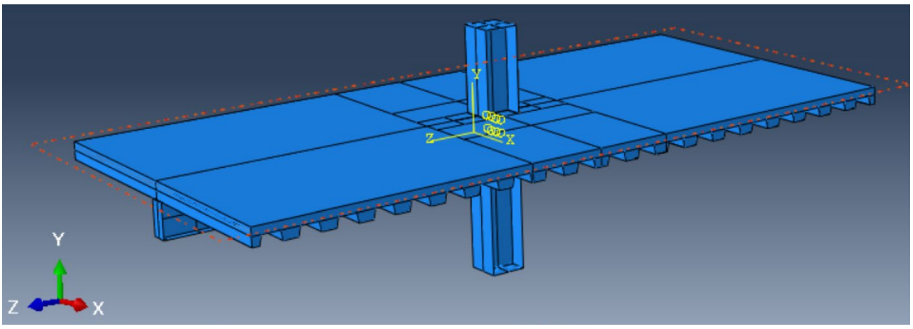

(b) Schematic of Tested Frame Sub-assembly.

Fig. 3 Details of finite element model

Table 1 CDP model material parameters

ψ	ϵ	f_{b0}/f_{c0}	k_c
13°	0.1	1.16	2/3

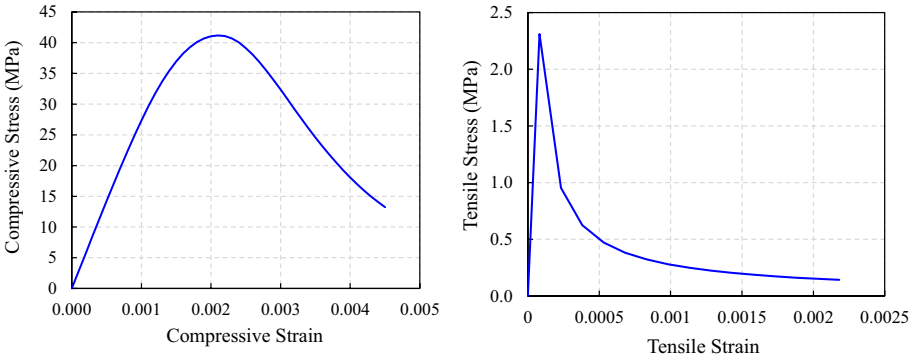

(a) Compression Envelope Curve **(b)** Tension Envelope Curve

Fig. 4 Uniaxial stress–strain curve of concrete under compression and tension loading

Material nonlinearity was incorporated by utilising the nonlinear constitutive law at the stress–strain level, geometric nonlinearities were assigned using 'Nlgom' feature available in ABAQUS software, and the interface nonlinearity associated with the contact opening and closing between the column and the slab was simulated using the 'contact pair' feature. A displacement control test protocol, with increasing lateral drift, was applied at the column top.

3.2 Material properties

3.2.1 Concrete

Concrete material was modelled using the concrete damage plasticity (CDP) model (Simulia 2011). Dilation angle (ψ), flow potential eccentricity (ϵ), ratio of initial biaxial compressive yield stress to initial uniaxial compressive yield stress (f_{b0}/f_{c0}), and ratio of second stress invariant on the tensile meridian to the compressive meridian at initial yield (k_c) were considered following Jankowiak and Lodygowski (Jankowiak and Lodygowski 2005). In the absence of sufficient relevant tests to identify all parameters, some values from the literature (Alfarah et al. 2017), reported in Table 1, were used.

Aslani and Jowkarmeimandi (Aslani and Jowkarmeimandi 2012) concrete uniaxial compression model was used; where the compression envelope is based on Carreira and Chu (Carreira and Chu 1985), with exponential values for the ascending and descending branches and compressive stress provided as a tabular function of plastic strain. The uniaxial compressive stress–strain curve was assumed linear up to $0.4f'_c$. Thereafter it was calculated according to Eqs. (1)–(3), as shown in Fig. 4a.

$$f_c = \frac{f_c' n\left(\frac{\varepsilon_c}{\varepsilon_c'}\right)}{n - 1 + \left(\frac{\varepsilon_c}{\varepsilon_c'}\right)^n} \tag{1}$$

$$n = n_1 = \left[1.02 - 1.17\left(E_{sec}/E_c\right)\right]^{-0.74} \text{ if } \varepsilon_c \le \varepsilon_c' \tag{2}$$

$$n = n_2 = n_1 + (a + 28b) \text{ if } \varepsilon_c \ge \varepsilon_c' \tag{3}$$

where f_c = Concrete compressive stress (MPa), E_c = Tangent modulus of concrete stress–strain curve (MPa), E_{sec} = Secant modulus of elasticity (MPa), ε_c = Concrete strain.

f'_c = Concrete cylinder compressive strength (MPa), ε'_c = Tensile strain corresponding to tensile strength = $\left(\frac{f_c'}{E_c}\right)\left(\frac{r}{r-1}\right)$, n = Material parameter depending on stress–strain curve shape, n_1 = Modified material parameter for ascending branch, n_2 = Modified material parameter for descending branch, a = Constant = $3.5\left(12.4 - 0.0166 f_c'(\text{MPa})\right)^{-0.46}$, b = Constant = $0.85exp\left(-911/f_c'(\text{MPa})\right)$, r = Constant = $\left(f_c'(\text{MPa})/17\right) + 0.8$

The stress–strain relationship of concrete under tension was assumed to be linear up to the concrete maximum tensile stress (tensile strength), f_{tu}, where f_{tu} (MPa) = $0.36\sqrt{(f'_c}$ (MPa)) (NZS3101:1 2006). Thereafter the tensile stress decreased, as shown in Fig. 4b. The concrete tensile stress–strain model is given in Eq. 4 (Aslani and Jowkarmeimandi 2012), where f_t is the concrete tensile stress, ε_t is the concrete tensile strain, f_{tu} is concrete tensile strength, and ε_{tu} is the strain corresponding to concrete maximum tensile strength.

$$\begin{aligned} f_t &= E_c \varepsilon_t \quad if \quad \varepsilon_t < \varepsilon_{tu} \\ &= f_{tu}\left(\varepsilon_{tu}/\varepsilon_t\right)^{0.85} \quad if \quad \varepsilon_t > \varepsilon_{tu}. \end{aligned} \tag{4}$$

3.2.2 Steel

The mechanical properties of the structural steel, such as nominal tensile stress (σ_{nom}) and nominal tensile strain (ε_{nom}) were obtained from the tension coupon tests (Chaudhari 2018). Nominal stress and strain properties were converted into true stress (σ_{true}) and strain ($\varepsilon^p{}_{true}$) using Eq. 5 and 6 to obtain Fig. 5:

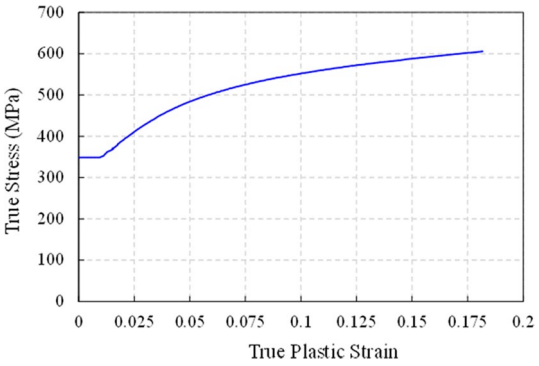

Fig. 5 Ture stress–strain curve of the structural steel

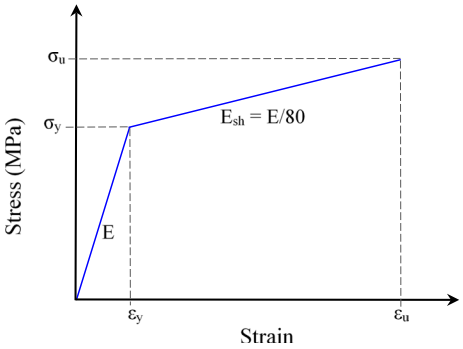

Fig. 6 Bilinear stress–strain curve for rebar and metal deck

Table 2 Rebar and Metal Deck Material Properties

Description		Yield stress (MPa)	Ultimate strength (MPa)	Modulus of elasticity (MPa)	Poisson's ratio
Rebar	Grade 300E	320	410	200,000 (NZS3101:1 2006)	0.3
	Grade 500E	515	659		
Metal deck sheet		500	640	205,000 (NZS3404:Part1:1997 1997)	0.3

$$\sigma_{true} = \sigma_{nom}\left(1 + \varepsilon_{nom}\right) \tag{5}$$

$$\varepsilon^{p}_{true} = \ln\left(1 + \varepsilon_{nom}\right) - \left(\frac{\sigma_{true}}{E}\right) \tag{6}$$

The metal deck sheet and the rebars were modelled using a bilinear stress–strain relationship as shown in Fig. 6 (Liang et al. 2005; Prakash et al. 2011).

For the rebar material, the yield stress was based on the minimum values specified in AS/NZS:4671 (2001), whereas the yield stress of the metal deck sheet was obtained from the ComFlor80 (2014) catalogue. The ultimate strength and strain hardening modulus for the metal deck and rebar was considered equal to 1.28 times yield stress (i.e. $\sigma_u = 1.28\sigma_y$) and 0.0125 times the modulus of elasticity (i.e. $E_{sh} = E/80$) respectively (Mirza and Uy 2011; Smitha and Kumar 2013). Key properties are reported in Table 2.

3.2.3 Coordinate system and boundary conditions

The global coordinate system is shown in Fig. 7 with the X-axis representing the frame subassembly out-of-plane direction. The Y and Z-axes coincide with the longitudinal axes of column and beam, respectively. The column base was restrained against translation and rotation, except rotation was permitted about the X-axis. Similarly, to replicate the beam end support condition of the actual test, rotation was only permitted about the X-axis and translation along the Z-axis to represent the roller supports. Column top out-of-plane lateral movement was restrained. These boundary conditions were applied to the master

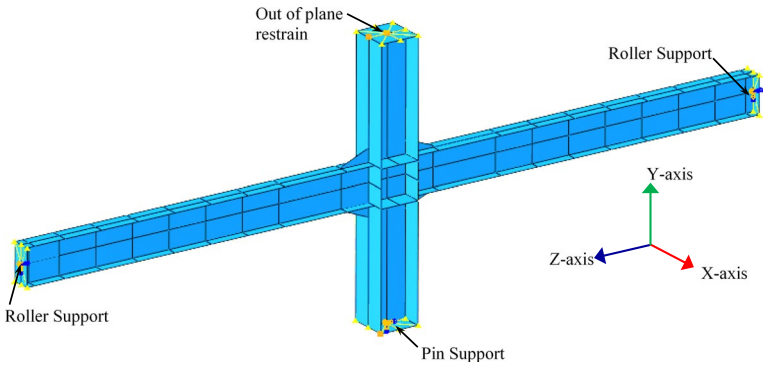

Fig. 7 Boundary condition

nodes at the column and beam end centre points. At these sections, to ensure plane sections remain plane, slave nodes with tie constraints followed the master node to achieve this as shown in Fig. 7.

3.2.4 Contact elements

3.2.4.1 Slab-column interaction The strength and stiffness of a composite frame subassembly depends on the degree of composite action between the slab and the beams, as well as on the robustness of the force transfer loadpaths (e.g. Fig. 2). To simulate the column-slab interaction, contact surfaces were assigned to the column flanges, web, endplate, gusset plates, and relevant slab surfaces. A surface-to-surface contact feature available in the ABAQUS was used to define the contact interaction between the column and the concrete slab. The desired interaction was achieved by providing a '*hard*' contact in the normal direction (to avoid the penetration into each other) and '*friction with penalty behaviour*' in the tangential direction (with a coefficient of friction of 0.2) (Salvatore et al. 2005; Gil and Bayo 2008). Note that the separation between the hard contacts was allowed under uplift. Column and gusset contact surfaces were modelled as master surfaces, and concrete slab surfaces were assigned as slave surfaces.

3.2.4.2 Slab-beam interaction In composite deck slabs, shear studs are provided to transfer longitudinal shear between the steel beam and deck slab thereby limiting the deck slip. Dowel action is the primary force transfer mechanism where the shear studs must sustain the slip induced at the steel and concrete element interface (Oehlers and Bradford 1995). In finite element modelling, the composite behaviour between the steel beam and composite slab is commonly simulated by either (i) modelling the shear stud as a 3D solid, or beam, element embedded into the concrete slab, or by (ii) using special elements like connectors/springs. However, the modelling of the shear studs as a 3D-solid element or beam element leads to increased computation time as well as difficulties in convergence (Henriques et al. 2013). In contrast, the employment of the spring elements (to simulate the composite action through the shear studs) is simple to use, gives good convergence, and is computationally more effective (Smitha and Kumar 2013; Gil and Bayo 2008; Henriques et al. 2013) (Wang and Tizani 2010). Hence, the non-linear shear springs were provided at each stud location to represent the stud behaviour in the horizontal and vertical directions.

The beam and the metal deck were modelled with a small gap between the beam top flange and the deck sheet in order to assign the shear spring. The spring connected the beam top flange node with the deck sheet node immediately below it at each shear stud location as shown in Fig. 8c. Beam flanges and deck sheets were modelled using shell elements with the middle surface as a reference plane. The gap between the beam top flange and the concrete slab is assumed to be equivalent to the summation of one-half of the thickness of the beam top flange and one-half of the thickness of the metal deck sheet (Baskar et al. 2002), as depicted in Fig. 8b. The node-to-node connection between metal sheet and steel beam top flange is achieved through the non-linear spring element representing the shear stud as shown in Fig. 8c.

The shear stud force–displacement relationship followed the Johnson and Molenstra (Johnson and Molenstra 1991) formulation in Eq. 7 where 'P_{rk}' is the characteristic strength of the shear studs of 39kN and 48kN for transverse and longitudinal deck respectively (Chaudhari 2018; Hicks 2011), and the values for constants 'α' & 'β' were selected as 0.989 and 1.535 mm^{-1} respectively Johnson and Molenstra (Johnson and Molenstra 1991).

$$P = P_{rk}(1 - e^{-\beta s})^{\alpha} \tag{7}$$

The shear stud non-linear load-slip behaviour shown in Fig. 8d was assigned to the nonlinear shear spring. The metal deck and beam flange nodes to which the spring connects are constrained against relative movement in the vertical and out-of-plane horizontal directions, and the rotational directions. In terms of decking-beam top flange

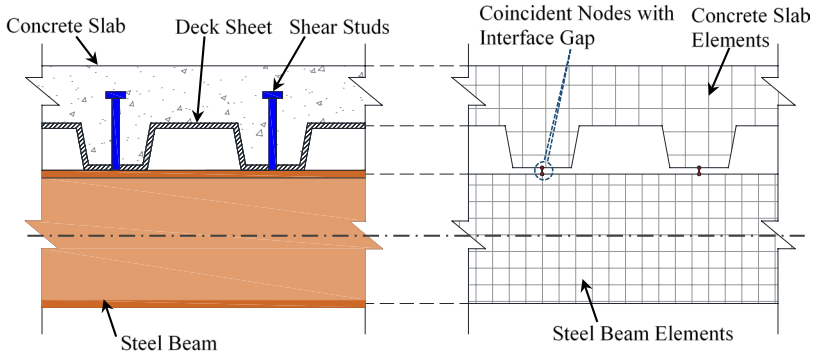

(a) Shear Studs in Tested Composite Beam

(b) Shear Studs in Finite Element Model

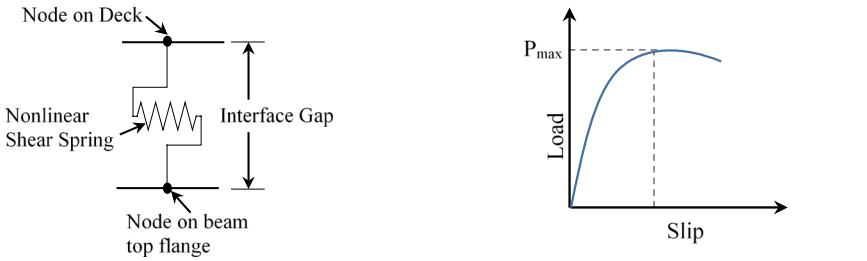

(c) Stud Idealisation as Nonlinear Shear Spring

(d) Shear Stud Load-Displacement Behaviour

Fig. 8 Shear stud schematic representation

lateral behaviour, both the slip relation at the studs, and the friction at the other nodes, contribute.

3.2.4.3 Deck – slab and Rebar-slab interaction The concrete slab and the metal deck were assumed to have a perfect bond, without uplift or slip for simplicity. This was realised by embedding the deck sheet into the concrete slab using the ABAQUS constraint option. Similar interaction was made for the rebars which were embedded into the concrete slab (Alashker et al. 2010).

3.2.5 Elements and meshing

The eight noded solid elements (C3D8R) with the reduced integration points were adopted to model the concrete slab to capture the concrete local failure (Salvatore et al. 2005; Prakash et al. 2011; Mirza and Uy 2011; Gil and Bayo 2008). The frame sub-assembly structural elements such as beams, column, gusset plates, column continuity plates and metal deck were modelled using four noded (S4R) shell elements with reduced integration points (Smitha and Kumar 2013; Alashker et al. 2010; Sadek et al. 2008) using auto-meshing. This resulted in less processing time compared to solid elements (Kim 2003; Broekaart 2016). Different mesh sizes were modelled to investigate the sensitivity effect on the overall global response of the frame sub-assembly with increasing lateral drift. The mesh sensitivity of the shell elements (S4R) was performed on the Bare Steel Frame (BSF) sub-assembly model with three different mesh sizes 20 mm (BSF-Mono-Mesh 20), 30 mm (BSF-Mono-Mesh 30) and 40 mm (BSF-Mono-Mesh 40). Whereas the mesh sensitivity of the solid elements (C3D8R) was performed on the Fully Isolated Slab Unit (FISU) sub-assembly model with three different mesh sizes 50 mm (FISU-Mono-Mesh 50), 75 mm (FISU-Mono-Mesh 75) and 100 mm (FISU-Mono-Mesh 100). Mesh sizes of 30 mm and 75 mm were selected to eliminate mesh sensitivity effects for steel (Shell elements, S4R) and concrete (Solid elements, C3D8R) components respectively, as shown for the frame sub-assembly global force-drift responses in Fig. 9.

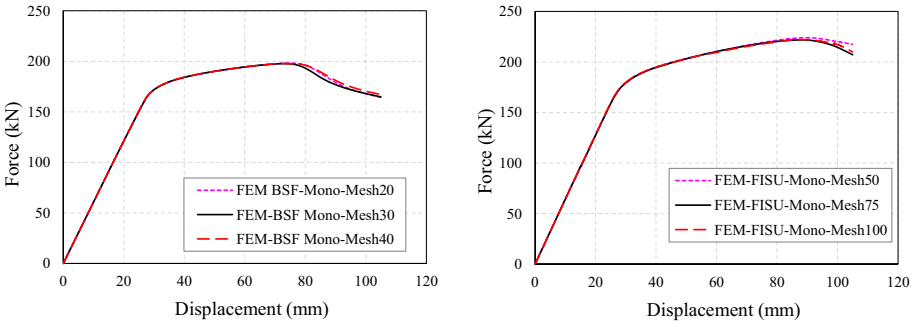

(a) Mesh Sensitivity: Shell Element (S4R) **(b)** Mesh Sensitivity: Solid Element (C3D8R)

Fig. 9 Mesh sensitivity analysis: load–displacement curves

3.2.6 Boundary conditions and test protocol

Beam ends were provided with vertical roller supports, and the column bottom with a pin support, to replicate the tested frame subassembly boundary conditions. Beam and column ends were restrained against out-of-plane displacement. The displacement control test protocol of Fig. 10 (specified in ACI T1.1-01 (2001)) was applied to the column top as per the experimental tests.

4 Numerical validation

As part of the experimental research, beam-column subassembly tests with different slab configurations were conducted at the University of Canterbury (Chaudhari 2018; Chaudhari et al. 2019). The four types of tested composite slab configurations are: (i) Fully Isolated Slab Unit (FI-SU), (ii) Shear Key Slab Unit (SK-SU), (iii) Modified Shear Key Unit (MSK-SU), and (iv) Full Depth Slab Unit (FD-SU). To investigate the contribution of the composite slab to the over-strength capacity of the beam, a bare steel frame (BSF) subassembly was also tested, which act as benchmark test. Specimen details are summarised in Table 3 and shown in Fig. 11.

The numerical monotonic force–displacement response and stiffness/strength values are compared with the experimental results shown in Fig. 12 and Table 4. The numerical model initial lateral stiffness is up to 17% greater than the experimental values where slip at the boundary element pins may occur. The strength was generally less than 3% different but it was almost 9% different for SK-SU. The numerical envelope follows the experimental hysteresis loop envelope for the BSF, FI-SU, and FD-SU frame sub-assemblies as depicted in Figs. 12a, b, and e, respectively. However, for the SK-SU frame sub-assemblies, where the decking was parallel to the main beam, the numerical model overpredicted the strength because the slab mid-height splitting/delamination failure mechanisms within the column flange region, which was noted during experimental test (Chaudhari et al. 2019), were not modelled in FEA.

Figures 13, 14, 15, 16, 17 show that the location and magnitude of the beam flange buckles compare well with the experiments. The simulated model could capture the buckling of the top and bottom flanges, and the location of the flange buckling in the numerical model matches with the experimental observations, although the buckle direction, which depends on the initial imperfections sometimes differed.

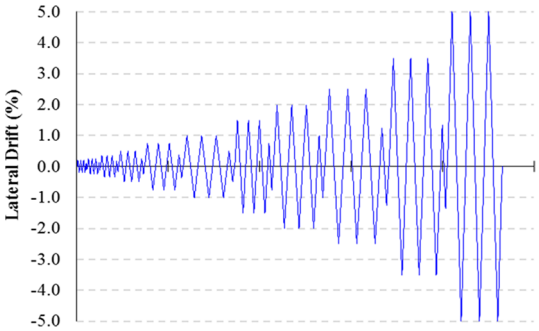

Fig. 10 Displacement control loading regime

Table 3 Details of experimental test configurations

Test	Specimen designation	Deck orientation	Detail around the column	Active force transfer mechanism
1	Bare Steel Frame (BSF)	–	–	–
2	Fully Isolated Slab Unit (FI-SU)	Transverse deck	All around isolation of slab from the column	None
3	Shear Key Slab Unit (SK-SU)	Longitudinal deck	Slab isolated on the column outer flange. U-shape shear key rebar	Mechanism-2
4	Modified shear key slab unit (MSK-SU)	Longitudinal deck	Slab isolated on the column outer flange. V-shape shear key rebar with anchorage and top confinement plates	Mechanism-2
5	Full depth slab unit (FD-SU)	Transverse deck	Slab casted touching to the column on full depth	Mechanism-1 and Mechanism-2

Fig. 11 Details of test sub-assemblies. **A** Bare steel frame (BSF) Test sub-assembly. **B** Fully isolated slab unit (FI-SU) Test sub-assembly. **C** Shear key slab unit (SK-SU) test sub-assembly **D** Modified shear key slab unit (MSK-SU) test sub-assembly. **E** Full depth slab unit (FD-SU) Test sub-assembly

The equivalent plastic strain distribution at 5.0% sub-assembly lateral drift is shown in Fig. 18, and it can be concluded that the column and the panel zone was in the elastic state, which was in line with the behaviour observed during the experimental tests conducted at the University of Canterbury (Chaudhari et al. 2019).

Figures 19, 20, 21, 22 show the minimum principal stress contour plots at the drift associated with the peak lateral strength from the numerical analysis. The minimum value represents slab compression. The isolated frame sub-assembly in Fig. 19 indicates low (< 4 MPa) slab compression because of slab isolation from the column, which deactivated the force transfer from the column to the slab. This matched the experimental behaviour (Chaudhari et al. 2019).

The shear key and modified shear key frame sub-assemblies, SK-SU and MSK-SU, were isolated at the column outer flanges to activate only the force transfer Mechanism 2 without force transfer Mechanism 1 as described in Fig. 1. As a result, little stress was observed on the outer side of the flanges as shown in Figs. 20 and 21 and the transfer Mechanism 2 forces are shown. The compression strut angle was approximately 45°, which is consistent with EN1998-1 (2004). The noted maximum compressive stress in the SK-SU and MSK-SU frame sub-assemblies was 22 MPa and 34 MPa, respectively, which lies between $0.6f_c'$ to $0.85f_c'$ (where $f_c' = 40$ MPa). This peak stress was locally concentrated at the tip of the column flanges, indicating the stress concentration on the sagging side of the beam. The average stress range in compression strut was around 15 MPa (i.e. $0.4f_c'$). The difference in the maximum compressive stress between the SK-SU and MSK-SU frame sub-assemblies was due to the different detailing (i.e. shear key rebars and the confined anchorage).

The compression stress field of the full depth frame sub-assembly in Fig. 22 was different to that of the other frame subassemblies because both force transfer mechanisms (i.e. Mechanism 1 and Mechanism 2) are active. The numerical model shows high stress levels in front of the column outer flanges (associated with the compression strut of Mechanism 1) and lower stress levels between the column flanges (associated with compression strut of Mechanism 2). Similar to the observations were made by Salvatore et al. (2005) and Mago and Clifton (2008). The maximum compression stresses in the Mechanism 1 and Mechanism 2 regions were 28 MPa and 18 MPa, respectively. These indicate $0.7f_c'$ and $0.45f_c$, where $f_c' = 40$ MPa, which is below the crushing stress, f_c', indicating no strength degradation from slab spalling is likely.

5 Analytical methodology

For conventional beam-column subassemblies with the slab cast up to the column which are subjected to lateral force, the beam-column-slab interaction develops internal forces as shown in Fig. 23. The internal slab force ($N_{s,L}$) centroid on the beam sagging side acts at the topping concrete mid-depth (i.e. $t_c/2$). Whereas on the hogging side, the concrete cracks and the internal slab force ($N_{s,R}$) acts at the rebar mesh elevation. This is the cover to the longitudinal mesh bars plus one-half of the mesh bar diameter, ϕ/2, from the top of the slab as shown in Fig. 22a.

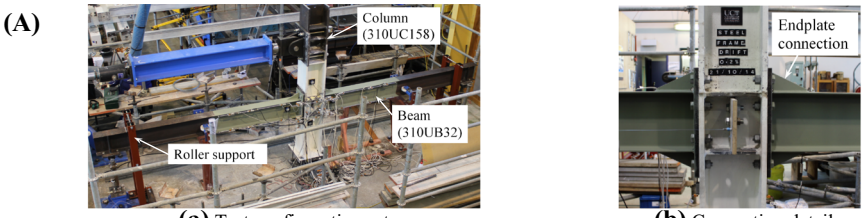

(a) Test configuration setup **(b)** Connection details

Bare Steel Frame (BSF) Test Sub-Assembly

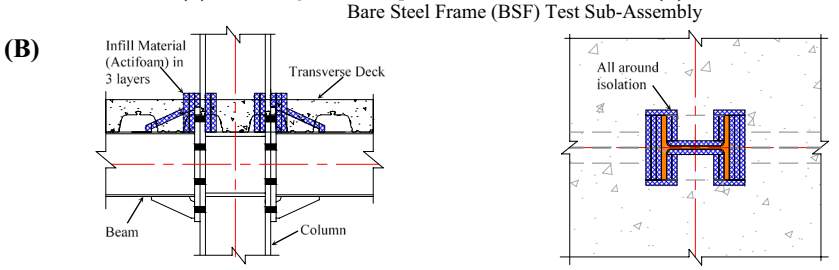

(a) Front view **(b)** Plan

Fully Isolated Slab Unit (FI-SU) Test Sub-Assembly

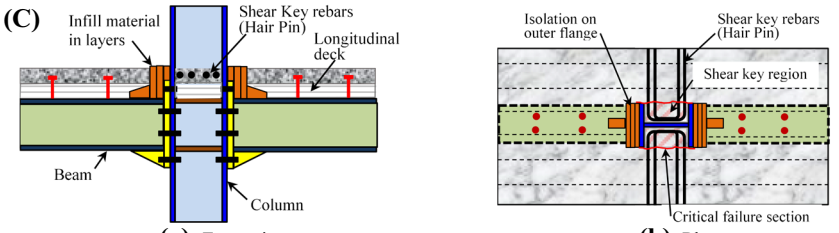

(a) Front view **(b)** Plan

Shear Key Slab Unit (SK-SU) Test Sub-Assembly

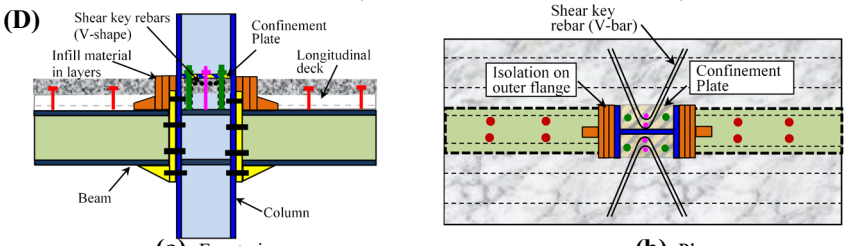

(a) Front view **(b)** Plan

Modified Shear Key Slab Unit (MSK-SU) Test Sub-assembly

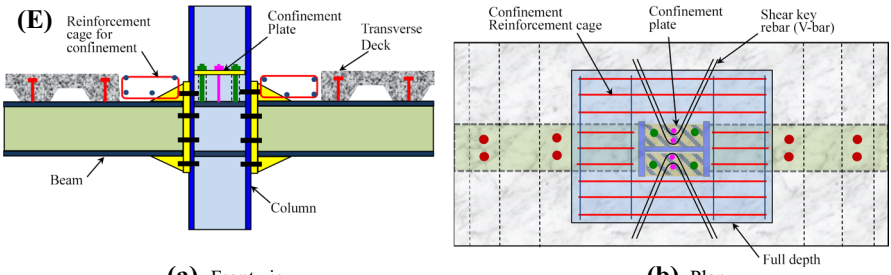

(a) Front view **(b)** Plan

Full Depth Slab Unit (FD-SU) Test Sub-Assembly.

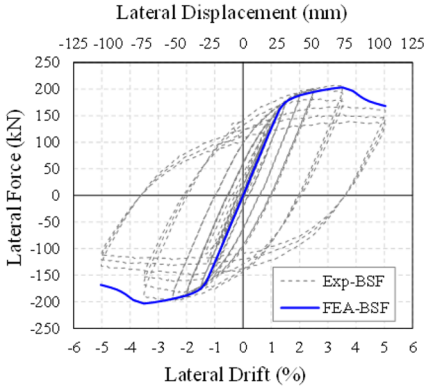

(a) Bare Steel Frame
(BSF: No Deck)

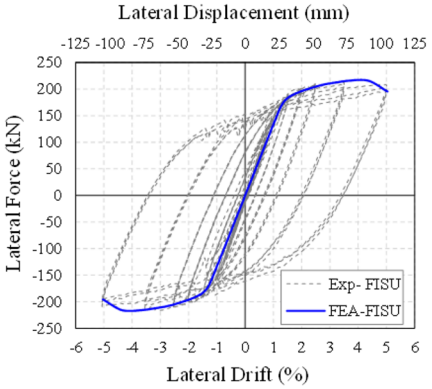

(b) Fully Isolated Slab Unit
(FI-SU: Transverse Deck)

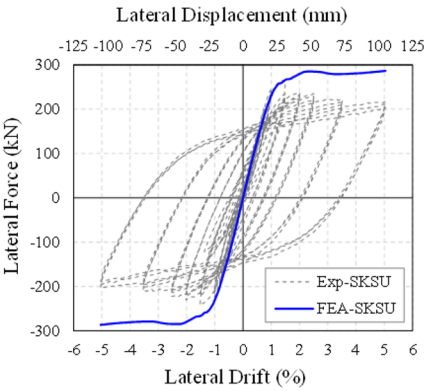

(c) Shear Key Slab Unit
(SK-SU: Longitudinal Deck)

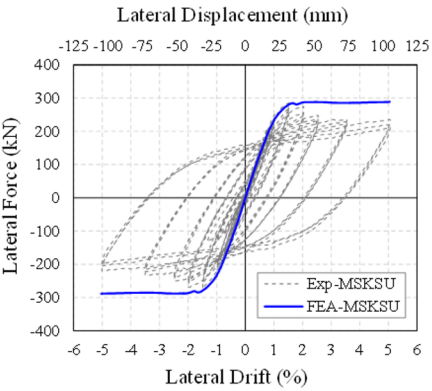

(d) Modified Shear Key Slab Unit
(MSK-SU: Longitudinal Deck)

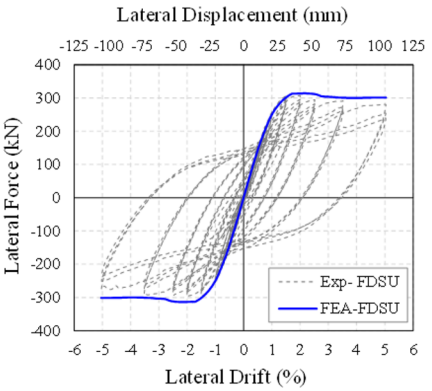

(e) Full Depth Slab Unit (FD-SU: Transverse Deck)

Fig. 12 Comparison of force–displacement of behaviour of numerically simulated result with the test results

Table 4 Comparison of Sub-assemblies initial stiffness and peak strength of numerical (FEA) model with experimental results

Test specimen	Initial stiffness (kN/m)			Peak strength (kN)		
	Numerical (FEA)	Experimental	Deviation (N-E)/E (%)	Numerical (FEA)	Experimental	Deviation (N-E)/E (%)
Bare steel frame (BSF)	6070	6156	− 1.4	203.1	206.0	− 1.4
Fully isolated slab unit (FI-SU)	7590	8747	− 15.2	217.3	211.4	2.7
Shear Key Slab Unit (SK-SU)	12,888	15,031	− 16.6	286.5	263.0	8.1
Modified shear key slab unit (MSK-SU)	13,137	14,506	− 10	288.6	285.2	1.2
Full depth slab unit (FD-SU)	14,136	16,402	− 16	313.7	306.3	2.4

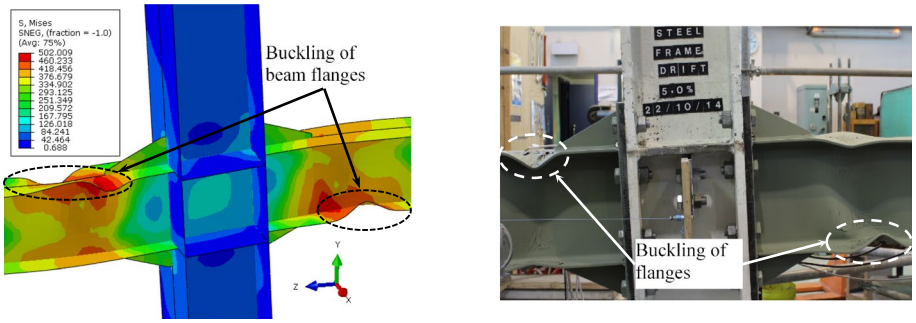

(a) Numerical (with Stress Contours) **(b)** Experimental

Fig. 13 Beam flange local buckling: BSF subassembly at 5.0% drift

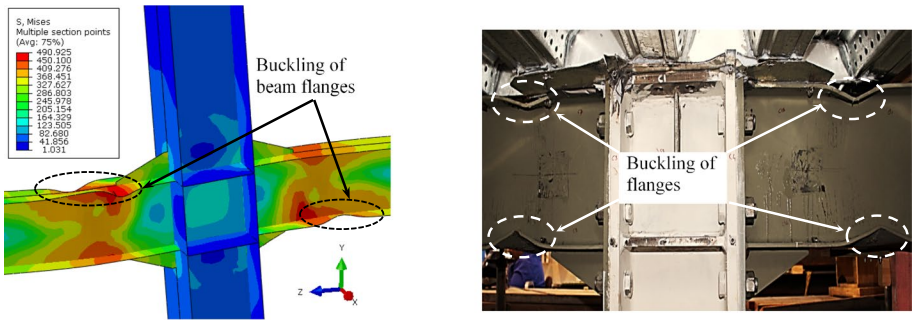

(a) Numerical (with Stress Contours) **(b)** Experimental

Fig. 14 Beam flange local buckling: FI-SU subassembly at 5.0% drift

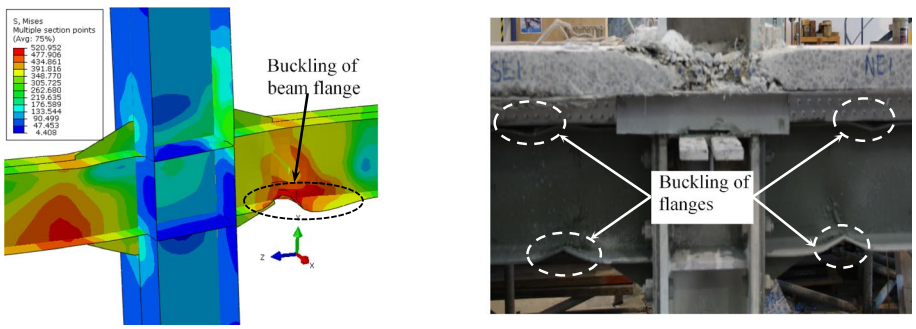

(a) Numerical (with Stress Contours) **(b)** Experimental

Fig. 15 Beam flange local buckling: SK-SU subassembly at 5.0% drift

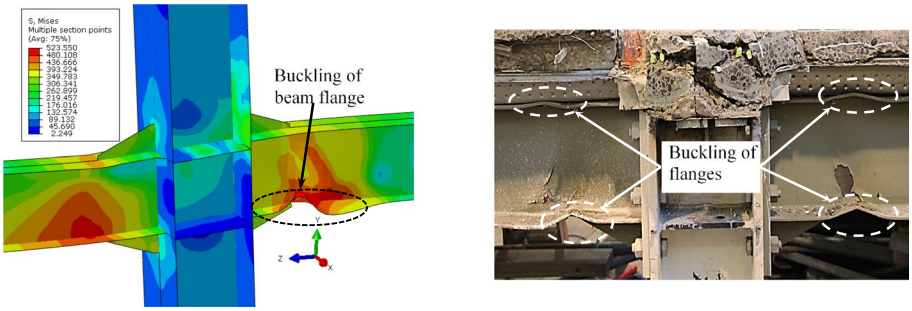

(a) Numerical (with Stress Contours) **(b)** Experimental

Fig. 16 Beam flange local buckling: MSK-SU subassembly at 5.0% drift

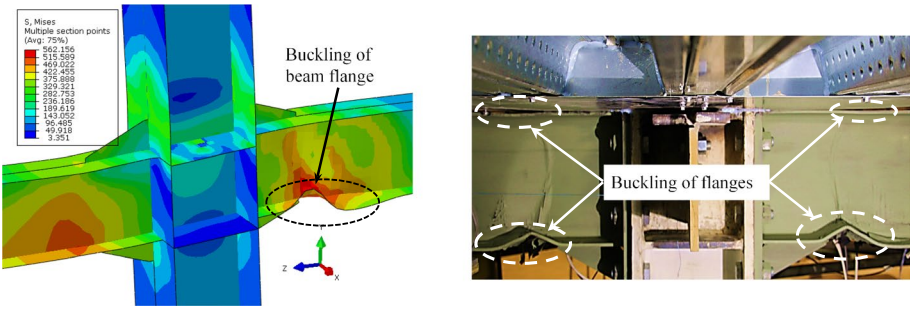

(a) Numerical (with Stress Contours) **(b)** Experimental

Fig. 17 Beam flanges local buckling: FD-SU subassembly at 5.0% drift

Treating the slab left- and right-hand sides separately, the total slab compression forces in the steel and concrete on the sagging (left) side, and the tension forces on the hogging (right) of the frame sub-assembly may be evaluated using the following equations:

$$N_{s,L} = min\begin{cases} Left\ Side\ Shear\ Stud\ Strength\left(F_{studs} = n_{sl}.P_{rk}\right) \\ Concrete\ Compressive\ Strength\ \left(F_{conc} = 0.85f_c^{'} \cdot b_{eff} \cdot t_c\right) \\ Steel\ Beam\ Strength\ \left(F_{steel} = A_g \cdot f_y\right) \end{cases} \tag{8}$$

$$N_{s,R} = min\begin{cases} Right\ Side\ Shear\ Stud\ Strength\left(F_{studs} = n_{sr} \cdot P_{rk}\right) \\ Rebar\ Strength\left(F_{rebar} = n_{\emptyset} \cdot A_{\emptyset} \cdot f_{y\emptyset}\right) \\ Steel\ Beam\ Strength\left(F_{steel} = A_g \cdot f_y\right) \end{cases} \tag{9}$$

where P_{rk} is characteristic strength of the shear stud, n_{sl} and n_{sr} are the number of beam shear studs in the subassembly on the left and right side of the column respectively, f'_c concrete compression strength, b_{eff} is the composite slab effective width, t_c is the composite slab topping thickness), A_g is the steel beam area framing into the column, f_y is yield strength of the steel beam flange, n_{ϕ} is number of rebars within the concrete slab effective

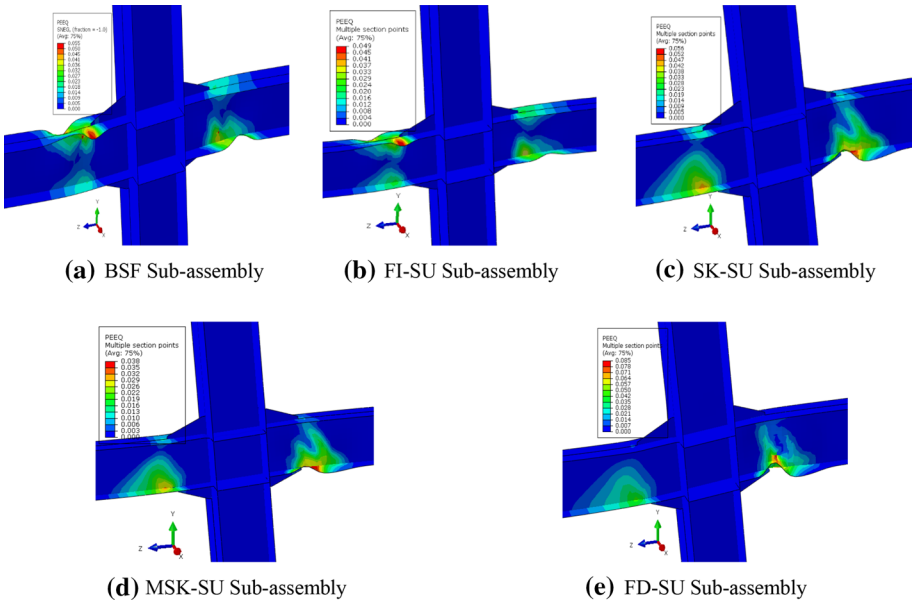

Fig. 18 Equivalent plastic strain at 5.0% lateral drift

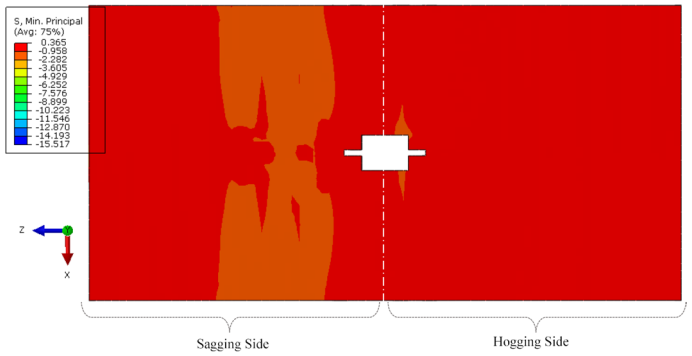

Fig. 19 Minimum principal stress contour at 3.5% drift: FI-SU sub-assembly

width, A_ϕ is the individual rebar area of and $f_{y\phi}$ is yield strength of the rebar. The splitting resistance of the concrete in front of the shear studs was checked as per HERA (Raed et al. 2003) and was found not to govern.

The force transferred from the slab directly to the column outer flanges, F_{rd1}, column (Mechanism 1) and from the slab to the column sides using the inclined concrete struts, F_{rd2}, from Mechanism 2 is shown in Fig. 22b, The resistance offered by Mechanism 1 can be related to the crushing strength of the concrete (Braconi et al. (Braconi et al. 2010)) using Eq. (10) (reproduced from EN1998-1 (EN1998-1 2004)):

$$F_{rd1} = 0.85 f_c^{'} \times B_c \times t_c \tag{10}$$

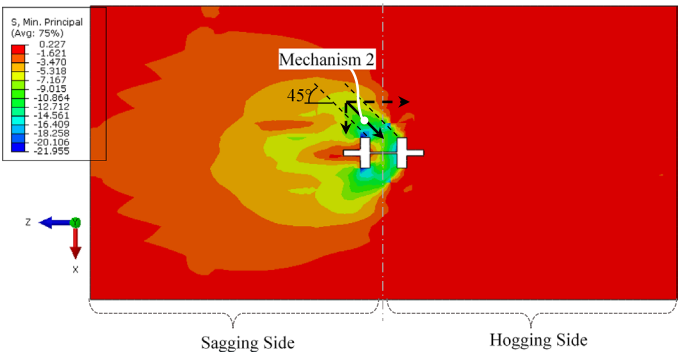

Fig. 20 Minimum principal stress contour at 1.5% drift: SK-SU sub-assembly

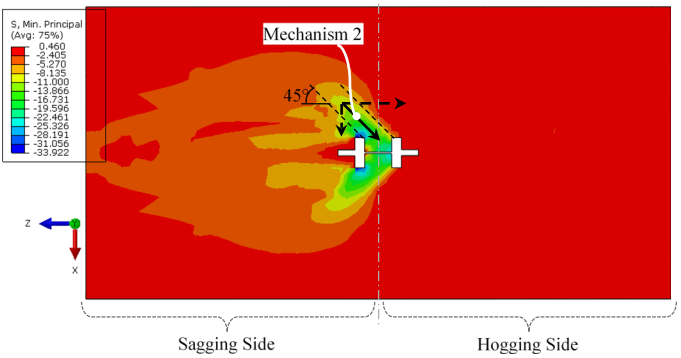

Fig. 21 Minimum principal stress contour at 1.5% drift: MSK-SU Sub-assembly

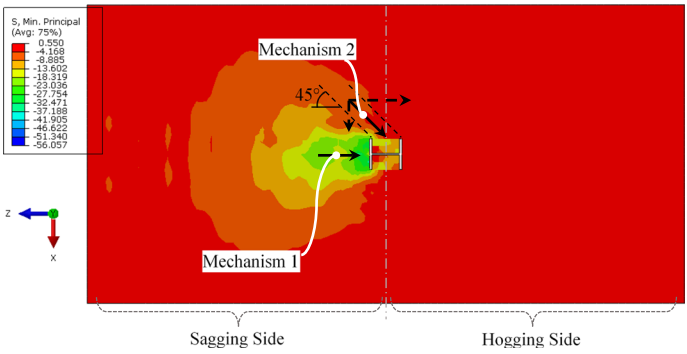

Fig. 22 Minimum principal stress contour at 2.0% drift: FD-SU sub-assembly

The strength associated with the force transfer Mechanism 2 was developed through the formation of two compressive struts on the column sides, which is shown in Fig. 22b considering the inclination angle of 45° (EN1998-1 2004) as shown in Fig. 24.

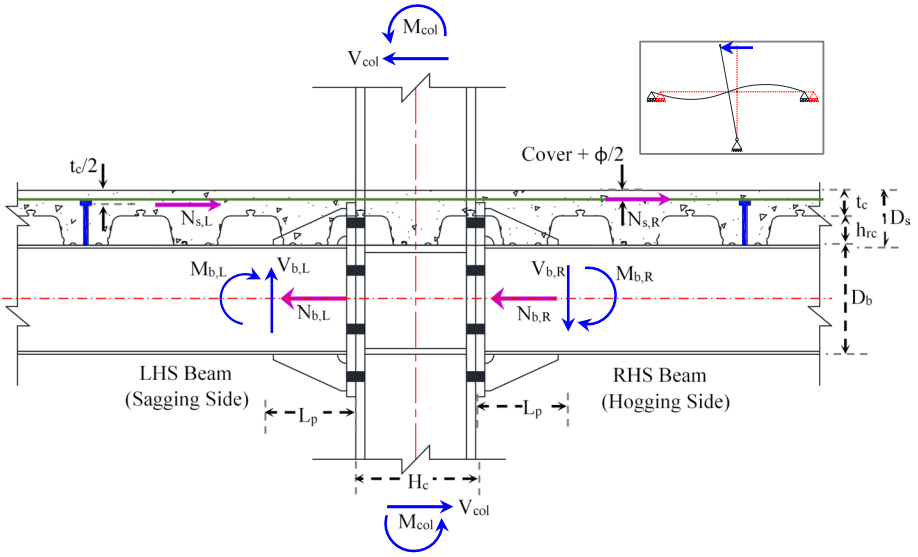

(a) Forces on the Joint

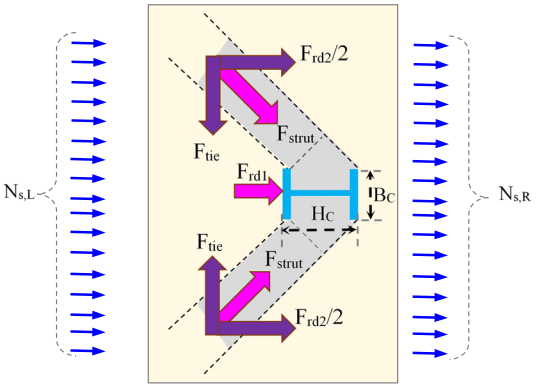

(b) Forces in the Slab-Column Interaction Zone

Fig. 23 Forces in the beam-column sub-assembly

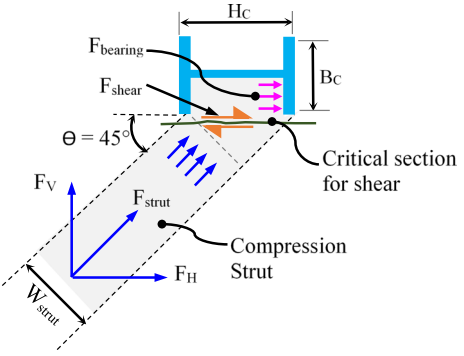

Fig. 24 Schematic representation of force transfer mechanism 2

Mechanism 2 compressive struts are analogous to the inclined struts formed in reinforced concrete deep beams in strut-and-tie theory. Column side interaction forces depends on the (i) bearing force developed on the internal column flanges, (ii) slab shear capacity between column flange tips, and (iii) compression strut capacity. The compression strut width (W_{strut}) was calculated as:

$$W_{strut} = H_c \cos\theta \tag{11}$$

The compression strut force was calculated using Eq. 12.

$$F_{strut} = \upsilon \times 0.85 f_c^{'} \times W_{strut} \times t_c \tag{12}$$

The compression strut's horizontal and vertical force components (F_H and F_V) on each side of the column are given by Eqs. (13) and (14), respectively where υ is the reduction factor (Plumier and Doneux 2001; EN1998-1 2004), and W_{strut} is the compressive strut width.

$$F_H = F_{strut} \cos\theta = \left(\upsilon \times 0.85 f_c^{'} \times W_{strut} \times t_c\right) \cos\theta \tag{13}$$

$$F_V = F_{strut} \sin\theta = \left(\upsilon \times 0.85 f_c^{'} \times W_{strut} \times t_c\right) \sin\theta \tag{14}$$

The shear resistance (F_{shear}) at the critical section (between column flange tips as shown in Fig. 23) was calculated using the shear friction method where μ is the friction coefficient of 1.4 for normal density concrete and N^* is the force acting perpendicular to the shear plane ($=F_V$). Mesh bar shear resistance was not considered here since it may be cut in this zone for construction ease. However, the shear resistance/capacity at this critical section, F_{shear}, may be enhanced by providing shear key rebars (Chaudhari et al. 2019) with area, A_v, yield strength, $f_{y\phi}$, and α is the angle between shear-friction reinforcement and shear plane as shown in Eq. (15) (NZS3101:1 2006).

$$F_{shear} = A_v f_{y\phi}(\mu \sin\alpha + \cos\alpha) + N^* \mu \tag{15}$$

The internal column flange force resistance on one side of the column $F_{bearing}$, is given in Eq. 16 where B_c is the column flange width, and t_{wc} is the column web thickness.

$$F_{bearing} = 0.85 f_c^{\prime} \times \left(\frac{B_c - t_{wc}}{2}\right) \times t_c \tag{16}$$

The Mechanism 2 force resistance (F_{rd2}) is governed by the minimum strength of the; (i) compressive strut horizontal force component, F_H, (ii) shear resistance at the critical section, F_{shear}, and, (iii) bearing resistance at the internal column flange, $F_{bearing}$, as shown in Eq. 17, where the factor of 2 indicates that the strength may come from both sides of the web.

$$F_{rd2} = min\begin{cases} 2 \cdot F_H \\ 2 \cdot F_{shear} \\ 2 \cdot F_{bearing} \end{cases} \tag{17}$$

Force transfer Mechanism 3 was developed through the interaction of the shear studs (installed on the secondary beam) and the concrete. The compression force developed from

the shear studs was transferred to the column through shear and twisting of the transverse beam (Plumier and Doneux 2001). Figure 25 pictorially explains the slab force transfer Mechanism 3 from the transverse beam to the column.

The internal force associated with mechanism-3 was calculated based on the recommendations specified by EC8 (EN1998-1 2004), given by Eq. (18).

$$F_{rd3} = n_{s\_tr} \times P_{rk} \tag{18}$$

where 'n_{s_tr}' is a number of shear studs installed within the effective width on the transverse beam. The additional in-plane moment demand on the column panel zone due to Mechanism 3 is calculated as:

$$M_{rd3} = F_{rd3}\left(\frac{D_{bs}}{2} + D_s - \frac{t_c}{2}\right) \tag{19}$$

At the slab-column interaction, the total interaction force (F_{int}) developed due to Mechanism 1 (F_{rd1}), Mechanism 2 (F_{rd2}), and Mechanism 3 (F_{rd3}) was calculated as the summation of the individual forces as given below:

$$F_{int} = F_{rd1} + F_{rd2} + F_{rd3} \tag{20}$$

The governing slab force is a minimum of the internal force developed in the composite section and the force developed due to the Mechanisms 1, 2 and 3, which is given by the following equation:

$$N_{slab} = minimum\ of \begin{Bmatrix} F_{\text{int}} \\ N_{sL} + N_{sR} \end{Bmatrix} \tag{21}$$

The total moment acting at the column centre ($M_{col,\ CL}$) accounting for the beam and slab effect was calculated as:

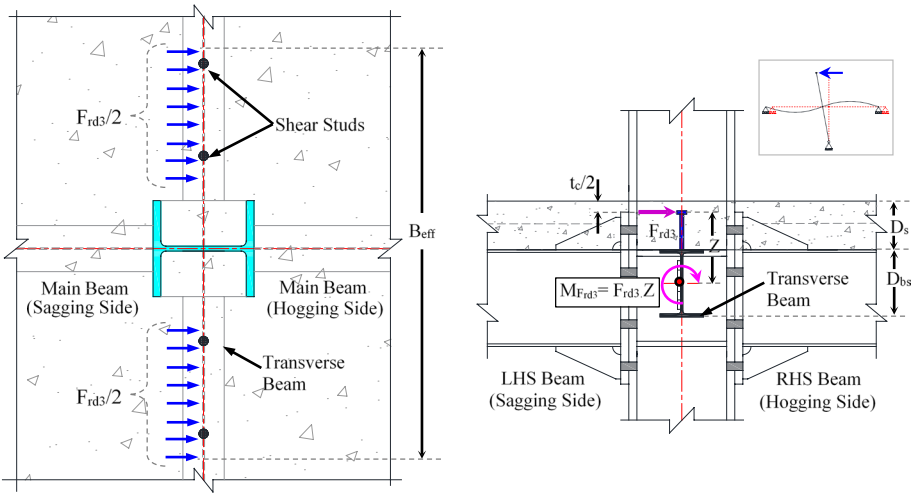

(a) Plan View **(b)** Sectional Elevation View

Fig. 25 Slab force transfer on the transverse beam (mechanism 3)

$$M_{col,CL} = M_{pb,L} + M_{pb,R} + N_{slab}\left(\frac{D_b}{2} + D_s - \frac{t_c}{2}\right) + V_{b,R}\left(\frac{D_c}{2} + L_p\right) + V_{b,L}\left(\frac{D_c}{2} + L_p\right) + F_{rd3}\left(\frac{D_{bs}}{2} + D_s - \frac{t_c}{2}\right) \tag{22}$$

In the above equations, the beam moments ($M_{pb,L}$ & $M_{pb,R}$) are modified to consider the axial-moment interaction as per NZS3404:Part1:1997 (NZS3404:Part1: 1997), the modified beam moments for the sagging and hogging sides are calculated assuming that the slab axial force is applied equally to the steel beams on both sides (with $N_{slab}/2$ on each side), as:

$$M_{pb,\ L} = \min\begin{cases} 1.18\left(1 - \left(N_{slab}/2\right)/A_{b,L}f_{y,L}\right)M_{b,L} \\ M_{b,L} \end{cases} \tag{23}$$

$$M_{pb,\ R} = \min\begin{cases} 1.18\left(1 - \left(N_{slab}/2\right)/A_{b,R}f_{y,R}\right)M_{b,R} \\ M_{b,R} \end{cases} \tag{24}$$

where $M_{pb,L}$ and $M_{pb,R}$ = Modified moment in left (sagging) and right (hogging) beam, respectively. $N_{b,L}$ and $N_{b,R}$ = Axial force in left and right beam respectively, $N_{b,L} = N_{s,L}$ and $N_{b,R} = N_{s,R}$. $A_{b,L}$ and $A_{b,R}$ = Cross-sectional area of left and right beam, respectively. $f_{y,L}$ and $f_{y,R}$ = Steel beam flange yield strength of the left and right beam, respectively. $M_{b,L}$ and $M_{b,R}$ = Beam maximum section moment capacity at the plastic hinge location in left and right beam respectively (Kawashima 1992; FEMA350, 2000; Bruneau 2011), $(f_y + f_u)/2$. Z_e.

The beam shear causing the maximum beam section moment capacity is given by:

$$V_{b,L} = \frac{M_{b,L}}{L_{b,L}} \text{and } V_{b,R} = \frac{M_{b,R}}{L_{b,R}} \tag{25}$$

where '$L_{b,L}$' and '$L_{b,R}$' are beam length between the tip of the gusset plate (where the plastic hinge forms), and the point of contraflexure for the left and right beam, respectively. The predicated maximum lateral strength at the column top ($V_{col,prd}$) is evaluated the story height (H) as:

$$V_{col,prd} = \frac{M_{col,CL}}{H}. \tag{26}$$

5.1 Validation of analytical results and discussion

The lateral strength of the frame subassemblies was estimated using the equations above. The lateral strength of the frame subassembly corresponding to the yield strength (f_y), average strength ($(f_y + f_u)/2$), and the ultimate strength (f_u) of the beam was calculated. Table 5 summarises the subassembly predicted lateral strength and compares it with the experimental results. The lateral strength corresponding to the yield and ultimate material strength of the beam provides the lower and upper bound values. It can be seen from Table 5 that the lateral strength calculated based on the beam average material strength was

Table 5 Comparison of predicted lateral strength of frame sub-assemblies with test results

Specimen description	Predicted lateral strength (kN)			Experimental lateral strength (kN)
	Lower bound based on yield strength (f_y)	Upper bound based on ultimate strength (f_u)	Average based on strength (f_y+f_u)/2	
Bare steel frame (BSF)	174	256	215	206
Fully isolated slab unit (FI-SU)	174	256	215	211
Shear key slab unit (SK-SU)	246	319	282	263
Modified shear key slab unit (MSK-SU)	253	322	287	285
Full depth slab unit (FD-SU)	250	321	285	306
Transverse deck slab unit (TD-SU) (Hobbs 2014)*	278	350	314	305
Longitudinal deck Slab Unit (LD-SU) (Hobbs 2014)*	314	379	346	361

*Test Units TD-SU and LD-SU were both tested by Hobbs (Hobbs 2014). Test LD-SU included a transverse beam with shear studs into the decking

in close agreement with the experimental test results. Based on the results summarised in Table 5, it was concluded that the proposed analytical methodology can reliably predict the lateral strength of the frame sub-assembly with different slab configurations. It also considers the strength hierarchy of the failure modes depicted in Fig. 1 and accounts for different force transfer mechanisms (i.e. Mechanism 1, 2 and 3).

The frame subassemblies considered represent the interior joint of a typical steel frame building. When the internal frame sub-assembly is subjected to lateral loads, it develops positive bending (i.e. sagging) in one beam and negative bending (i.e. hogging) in the other beam. This leads to different second moments of area on the sagging and hogging sides. Therefore, the subassembly initial lateral stiffness with a composite slab was calculated using an equivalent moment of inertia (I_{eq}), which takes into account the effective moment of inertia on the sagging and hogging sides, which is given by Eq. (27) (EN1998-1 2004; Cowie 2015):

$$I_{eq} = 0.6I_{eff\_sag} + 0.4I_{eff\_hogg} \tag{27}$$

The effective moment of inertia of the composite beam (I_{eff}) considering the effect of the degree composite action was calculated using Eq. (28) (NZS3404:Part1 1997):

$$I_{eff} = I_{st} + 0.85P_{comp}^{0.25}\left(I_{tr} - I_{st}\right) \tag{28}$$

where I_{eff_sag} and I_{eff_hogg} = Effective second moment of area of composite beam in positive (sagging) bending and negative (hogging) bending respectively. I_{st} = Second moment of area of steel beam alone. I_{tr} = Composite beam second moment of area transformed into an equivalent steel section. P_{comp} = Degree of composite action.

Comparisons of different subassembly predicted strengths and stiffnesses with the test results are shown in Fig. 26. Again, it may be seen that the experimental peak lateral strength falls within the predicted lower and upper bound values. Also, the proposed methodology reasonably predicts subassembly stiffness, as well as strength, for the different slab configurations but the stiffness does tend to be an upper bound as the model does not consider connection slip.

The column moment demand contribution due to beam and slab deformations is shown in Fig. 27. It was computed as the flexural strength without the slab effect, divided by the strength from all terms of the Eq. 26. The presence of the slab contributed around 30–44% of the column total moment demand, increasing the bare steel frame strength by 62–76%. For the isolated frame sub-assembly (FI-SU), the moment demands due to the slab were negligible due to the absence of the active force transfer mechanisms. For the longitudinal deck frame sub-assembly (LD-SU), all three force transfer mechanisms (1, 2, and 3) were active, and the moment demands due to the slab was the highest (i.e. around 44%), possibly due to the effect of Mechanism 3. Note that the steel beam contribution includes the axial (P)-moment (M) interaction, so the strength associated with the beam on specimens with a slab is not the same as that without the slab.

While the subassembly lateral strength with the composite deck slab was dictated by a number of active force transfer mechanisms, the two major parameters affecting subassembly lateral strength were; (i) the degree of composite action and (ii) the effectiveness factor (υ). A parametric study was conducted to evaluate the influence of these parameters on the subassembly lateral strength with different slab configurations.

The effect of the degree of the composite action (i.e. the number of shear studs) on the subassembly lateral strength is reported in Table 6. In the full depth frame sub-assembly (FD-SU), the lateral strength was increased by 10% for the full composite action, from

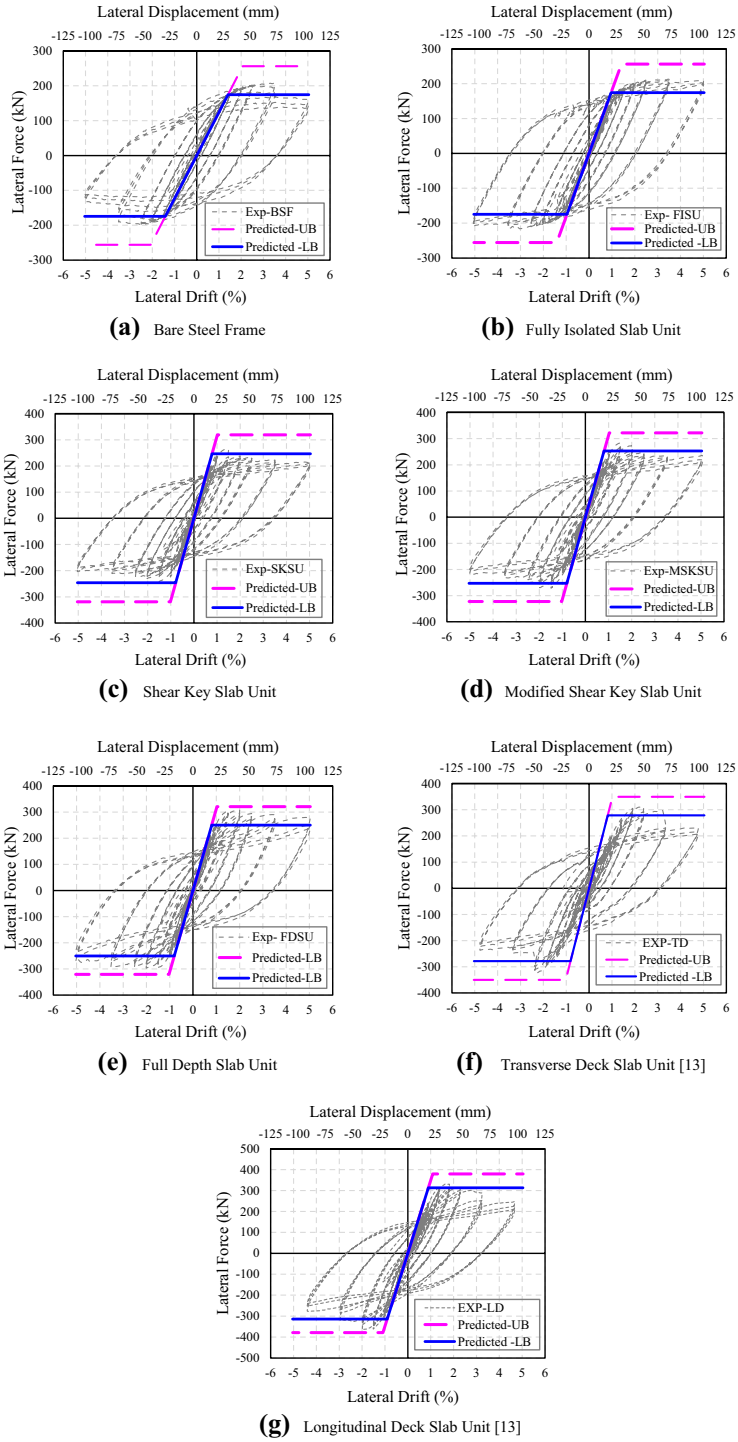

Fig. 26 Comparison of lateral strength and stiffness: predicted and experimental

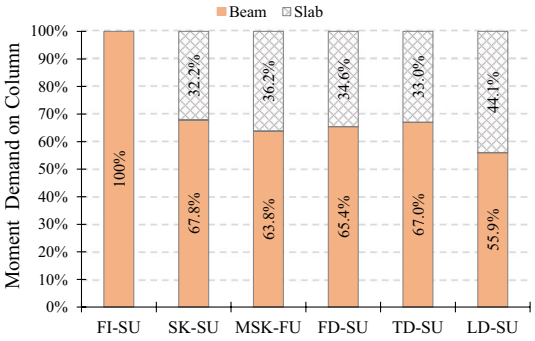

Fig. 27 Moment demand onto column due to beam and slab deformation

the case tested with 46% composite action. However, the lateral strength was limited by the stud shear strength and the governing force transfer mode (i.e. shear stud strength) remained the same irrespective of the degree of composite action. This was because the provision of full depth slab around the column enhances the strengths of the other modes. On the other hand, for the transverse deck and longitudinal deck frame subassemblies (TD-SU and LD-SU), the force transfer mode changes from shear stud strength (at 46% composite action) to the concrete crushing on the column flange (i.e. Modes 2 and 3 in Fig. 1) with the increase in the degree of composite action. The influence of the degree of composite action on the lateral strength was seen only in the FD-SU, TD-SU, and LD-SU frame sub-assemblies, wherein both the force transfer mechanism-1 and 2 were active. In the case of FI-SU frame sub-assembly were no active force transfer mechanisms, frame sub-assembly's lateral strength remains constant irrespective of the increase in the degree of composite action. Similar observations were made for the SK-SU and MSK-SU frame sub-assemblies, where only force transfer mechanism-2 was active. It can be concluded that the lateral strength of the frame sub-assembly depends on the number of active force transfer mechanisms and the strength associated with the individual component.

The compressive strength of the struts in Mechanism 2 depends on the effectiveness factor (υ) as shown in Fig. 24. It varies from 0.6 to 1.0 (Plumier and Doneux 2001; NZS3101:1 2006; Yun and Ramirez 1996). It's influence on subassemblies SK-SU and MSK-SU lateral strength, where only Mechanism 2 was active was about 5.0% when the effectiveness factor (υ) changed from 0.6 to 1.0 as shown in Fig. 28. For the subassemblies with both Mechanisms 1 and 2 active, the effect υ on the subassembly strength is negligible. It can be concluded that the effect of the effectiveness factor (υ) can be ignored for practical purposes.

6 Conclusions

Modelling was conducted of steel moment frame beam-column-joint subassemblies with different slab details which had been experimentally tested with a cyclic displacement regimes. A detailed finite element model incorporating contact and interaction elements, with plate elements for the steel, and solid elements for the concrete, was used. Furthermore, a simple analytical model suitable for design, was considered. It was shown that:

(i) The 3D finite element model considered the: steel characteristics; concrete characteristics; shear-stud characteristics; slab concrete crushing on column outer, and

Table 6 Composite action effect (P_{comp}) on subassembly lateral strength

Specimen description	Degree of composite action (P_{comp}) (%)	Predicted lateral strength (kN)	Governing force transfer mode (refer to Fig. 1)
Fully isolated slab unit (FI-SU)	46	215	Beam yielding
	75		
	100		
Shear key slab unit (SK-SU)	46	282	Mode 3: Concrete crushing on internal column flanges
	75		
	100		
Modified shear key slab unit (MSK-SU)	46	287	Mode 3: Concrete crushing on internal column flanges
	75		
	100		
Full depth slab unit (FD-SU)	46	285	Mode 1: Failure of shear stud
	75	301	
	100	315	
Transverse deck slab unit (TD-SU) (Hobbs 2014)	46	314	Mode 1: Failure of shear stud
	75	324	Mode 2 and Mode 3: Concrete crushing on column outer and internal column flanges
	100		
Longitudinal deck slab unit (LD-SU) (Hobbs 2014)	46	346	Mode 1: Failure of shear stud
	75	362	Mode 2 and Mode 3: Concrete crushing on column outer and internal column flanges
	100		

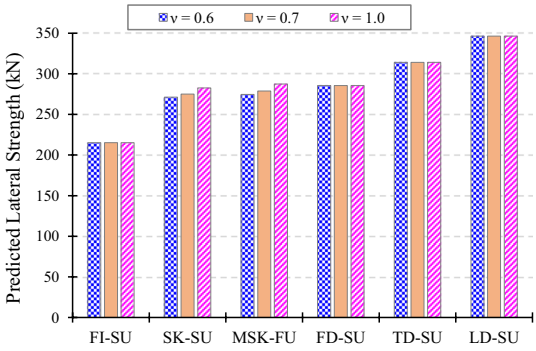

Fig. 28 Effect of effectiveness factor on the lateral strength of the frame sub-assembly

internal, flanges; the shear resistance between column flange tips; the compression resistance within the concrete decking; and transverse and longitudinal rebar yielding. The model, calibrated based on the steel and concrete properties and subjected to monotonic displacements, provided good global estimates of subassembly lateral force–displacement envelope curves for subassemblies with no slab, a gap between the concrete and steel column, and with a full depth slab. The numerical model initial lateral stiffness is up to 17% greater than the experimental values and the strength was less than 3% to 9%. Frame subassemblies with the concrete slab isolated from the column external flange, degraded in strength faster in the experiment than in the model as a result due to the model not capturing all failure modes. The equivalent plastic strain distribution at 5.0% sub-assembly lateral drift shows that the column and the panel zone was in the elastic state, which was in line with the behaviour observed in the experimental tests. The average contact pressure resulted due to slab-column interaction was found to be lower than the compressive strength of the concrete (f′c), and the localised contact pressure was higher than the average contact pressure, this was due to stress concentration.

(ii) The simple analytical design/assessment methodology, developed using the beam plastic moment capacity (considering axial-moment interaction) and the slab forces based on the strut-and-tie mechanism, evaluated the frame subassembly lateral strength and stiffness. It considered the parameters and deformation modes used for the FEM approach. Experimental test strength was always within the tolerances considering different assumptions about the material strengths, and the best estimate of strength had an accuracy of better than 7% for the comparisons made. Furthermore, the observed modes of failure were represented. The presence of a slab touching the concrete column increased the lateral strength by 30% to 44%. Based on the parametric study, the number of shear studs has negligible effect in case of FI-SU, and SK-SU and MSK-SU (with only one active mechanism) frame sub-assembly's strength, whereas in other frame sub-assemblies (i.e. FD-SU, TD-SU, and LD-SU), the effect of composite action varies, and it cannot be ignored. Hence the lateral strength of the frame sub-assembly depends on the number of active force transfer mechanisms and the strength associated with the individual component.

(iii) The mode of deformation affecting the strength, and failure mechanism varied, based on the relative properties of the different elements. All modes controlled in some cases.

(iv) For design, the analytical approach developed allows estimation of the key aspects of subassembly performance. It is fundamental in concept and easy to implement, encouraging engineers to detail appropriately to maintain load paths. The proposed

analytical model considers the effect of the composite deck slab with various construction detailing, deck orientation as compared to existing analytical model/methodology. It also considers the strength hierarchy of various nonlinear deformation modes of steel beam plastic hinging, concrete crushing both outside the column flange and within the beam flanges, slab shear fracture between the column flange tips, slab longitudinal and lateral reinforcement yielding as it carried the subassembly moments and transferred forces between the steel frame and the slab, and shear stud deformation. It improves existing NZS3404 methods for behaviour estimation. Slab effects, when the slab touches the column and shear studs are present, always cause an increase in demands on the column and panel zone which need to be considered as part of design. If there are no shear studs, or the column is isolated from the slab, there is no need to consider the slab effect in the column demands. If the slab is fully confined around the column, preventing slab degradation during the large inelastic deformations, then the composite slab strength can be considered to provide increased beam resistance, possibly allowing smaller steel beams to be used.

Acknowledgements The authors would like to acknowledge the MBIE Natural Hazards Research Platform for its support to conduct the proposed research study as a part of the Composite Solution Research Project. Additional support was provided by ComFlor New Zealand, John Jones Steel Research Funding, and Heavy Engineering Educational and Research Foundation (HEERF). All opinions expressed remain those of the authors.

Funding Open Access funding enabled and organized by CAUL and its Member Institutions. No funding was received to assist with the preparation of this manuscript.

Declarations

Conflict of interest The authors declare that they have no known competing financial interests or personal relationships that could have appeared to influence the work reported in this paper.

References

ACI (2001) ACI T1.1-01: Acceptance criteria for moment frames based on structural testing", American Concrete Institute

Alashker Y et al (2010) Progressive collapse resistance of steel-concrete composite floors. J Struct Eng 136(10):1187–1196

Alfarah B et al (2017) New methodology for calculating damage variables evolution in Plastic Damage Model for RC structures. Eng Struct 132:70–86

AS/NZS:4671 (2001) "Steel reinforcing materials", Standards New Zealand, Wellington

Aslani F, Jowkarmeimandi R (2012) Stress-strain model for concrete under cyclic loading. Mag Concr Res 64(8):673–685

Baskar K et al (2002) Finite-element analysis of steel-concrete composite plate girder. J Struct Eng-ASCE 128(9):1158–1168

Braconi A et al (2010) Seismic behaviour of beam-to-column partial-strength joints for steel–concrete composite frames. J Constr Steel Res 66(12):1431–1444

Broekaart D (2016) Simuleon FEA Blog - 5 reasons why you should use a mid-surface shell mesh for thin-walled parts available at "http://info.simuleon.com/blog/5-reasons-why-your-fea-simulations-should-be-setup-with-a-mid-surface-shell-mesh-for-thin-walled-parts"." (7 June 2017)
Bruneau M et al (2010) Preliminary report on steel building damage from the Darfield earthquake of September 4, 2010. Bull N Z Soc Earthq Eng 43(4):351–359
Bruneau M et al (2011) Ductile design of steel structures. McGraw Hill Professional
Carreira DJ, Chu KH (1985) Stress-strain relationship for plain concrete in compression. J Am Concrete Inst 82(6):797–804
Chaudhari T (2018) Seismic performance evaluation of steel frame building with different composite slab configurations. Doctor of Philosophy in Civil Engineering Ph.D. Thesis, University of Canterbury, Christchurch, New Zealand
Chaudhari T et al (2019) Experimental behaviour of steel beam-column subassemblies with different slab configurations. J Constr Steel Res 162:105699
Chaudhari T et al (2015) Composite slab effects on beam-column subassembly seismic performance. STESSA 2015, China Architecture and Building Press
Civjan SA et al (2001) Slab effects in SMRF retrofit connection tests. J Struct Eng 127(3):230–237
ComFlor80 (2014) "Product guide ComFlor80, available at "http://www.comflor.co.nz/wp-content/uploads/ComFlor/Brochures/ComFlor80Brochure.pdf"." (13 January 2014)
Cowie K (2015) Australian/New Zealand Standard for Composite Structures, AS/NZS 2327, Seismic Provisions Development. Steel Innovations Conference 2015, Steel Construction New Zealand
EN1998-1 (2004) Eurocode 8: Design of structures for earthquake resistance - Part 1: General rules, seismic actions and rules for buildings", European Committee for Standardization, B-1050 Brussels
FEMA350 (2000) Recommended design criteria for new steel moment frame buildings. Federal Emergency Management Agency, Washington
Gil B, Bayo E (2008) An alternative design for internal and external semi-rigid composite joints. Part II : Finite element modelling and analytical study. Eng Struct 30(1):232–246
Henriques J et al (2013) Numerical modeling of composite beam to reinforced concrete wall joints Part I : Calibration of joint components. Eng Struct 52:747–761
Hicks S (2011) Design resistances of 19 mm diameter headed stud connectors through-deck welded within the ribs of Comflor 60 and Comflor 80 profiled steel decking. HERA, Manukau City, New Zealand, (Received through private communication from Steve Stickland)
Hobbs M (2014) Effects of slab-column interaction in steel moment resisting frames with steel-concrete composite floor slabs. Master Thesis, University of Canterbury, Christchurch, New Zealand
Hobbs M et al (2013) Slab column interaction - significant or not? Steel Innovations, SCNZ
Jankowiak T, Lodygowski T (2005) Identification of parameters of concrete damage plasticity constitutive model. Found Civ Environ Eng 6(1):53–69
Johnson RP, Molenstra N (1991) Partial shear connection composite beams for buildings. Proc Inst Civ Eng 2:679–704
Kawashima K et al (1992) The strength and ductility of steel bridge piers based on loading tests. J Res Jpn, p 29
Kim T (2003) Experimental and analytical performance evaluation of welded steel moment connections to box or deep w-shape columns." Ph.D. Thesis, University of California, Berkeley
Lee S-J, Lu L-W (1989) Cyclic tests of full-scale composite joint subassemblages. J Struct Eng 115(8):1977–1998
Leon RT et al (1998) Seismic response of composite moment-resisting connections. I: Performance. J Struct Eng 124(8):868–876
Liang QQ et al (2005) Strength analysis of steel–concrete composite beams in combined bending and shear. J Struct Eng 131(10):1593–1600
MacRae G, Clifton G (2015) NZ research on steel structures in seismic areas. In: Proceedings of the 8th international conference on behavior of steel structures in seismic areas, STESSA, Shanghai, China, pp 44–58
MacRae GA et al (2007) Overstrength effects of slabs on demands on steel moment frames. Pacific structural steel conference 2007
MacRae G et al (2013) Slab effects on beam-column subassemblies—beam strength and elongation issues. Compos Construct Steel Concrete VII, pp 77–92
Mago N, Clifton CG (2008) Investigation of the slab participation in moment resisting steel frames (HERA report R 4–140). New Zealand Heavy Engineering Research Association, Manukau City, New Zealand
Mirza O, Uy B (2011) Behaviour of composite beam-column flush end-plate connection subjected to low-probability, high-consequence loading. Eng Struct 33:647–662
NZS3101:1 (2006) Concrete structures standard: Part 1 - The design of concrete structures", Standards New Zealand, Wellington

NZS3404:Part1:1997 (2007) Steel structures standard part 1-Incorporating amendment no 1 and no 2", Standards New Zealand, Wellington
Oehlers DJ, Bradford MA (1995) Composite steel and concrete structural members : fundamental behaviour. Elsevier, Kidlington, Oxford
Plumier A, Doneux C (2001) Seismic behaviour and design of composite steel concrete structures. ECOEST2 and ICONS, LNEC Lisboa, Portugal
Prakash A et al (2011) Three dimensional FE model of stud connected steel-concrete composite girders subjected to monotonic loading. Int J Mech Appl 1(1):1–11
Raed Z et al (2003) Shear Stud Capacity in Profiled Steel Decks. HERA Steel Design and Construction Bulletin (DCB No. 76)
Sadek F et al (2008) Robustness of composite floor systems with shear connections: modeling, simulation, and evaluation. J Struct Eng 134(11):1717–1725
Salvatore W et al (2005) Design, testing and analysis of high ductile partial-strength steel–concrete composite beam-to-column joints. Comput Struct 83(28):2334–2352
Simulia (2011) ABAQUS version 6.11. User's manual." Dassault Systemes
Smitha MS, Kumar SRS (2013) Steel-concrete composite flange plate connections - finite element modeling and parametric studies. J Constr Steel Res 82:164–176
Umarani C, MacRae G (2007) A new concept for consideration of slab effects on building seismic performance. J Struct Eng Struct Eng Res Centre Chennai India 34–3:34
Wang Z, Tizani W (2010) Modelling techniques of composite joints under cyclic loading. In: Computing in civil and building engineering, proceedings of the international conference, (Nottingham University Press, Nottingham, UK), Paper 254, p 507
Webb G et al (2018) Column moment demands from orthogonal beam twisting. Proc Key Eng Mater Trans Tech Publ, pp 259–269
Yamada S et al (2009) Full scale shaking table collapse experiment on 4-story steel moment frame: Part 1 outline of the experiment. Behav Steel Struct Seismic Areas: STESSA 2009:125
Yun YM, Ramirez JA (1996) Strength of struts and nodes in strut-tie model. J Struct Eng 122(1):20–29

Authors and Affiliations

Tushar Chaudhari[1] · Gregory MacRae[2] · Des Bull[2] · G. Charles Clifton[3] · Stephen J. Hicks[4]

Gregory MacRae
gregory.macrae@canterbury.ac.nz

Des Bull
des.bull@canterbury.ac.nz

G. Charles Clifton
c.clifton@auckland.ac.nz

Stephen J. Hicks
stephen.j.hicks@warwick.ac.uk

[1] Pune, India

[2] Department of Civil and Natural Resources Engineering, University of Canterbury, Christchurch, New Zealand

[3] Department of Civil and Environmental Engineering, University of Auckland, Auckland, New Zealand

[4] School of Engineering, University of Warwick, Coventry CV4 7AL, UK